High thermal stability of diamond–cBN–B_4C–Si composites*

Hong-Sheng Jia(贾洪声)[1], Pin-Wen Zhu(朱品文)[2,†], Hao Ye(叶灏)[1], Bin Zuo(左斌)[1], Yuan-Long E(鄂元龙)[1], Shi-Chong Xu(徐仕翀)[1], Ji Li(李季)[1], Hai-Bo Li(李海波)[1,‡], Xiao-Peng Jia(贾晓鹏)[2], and Hong-An Ma(马红安)[2]

[1] *Key Laboratory of Functional Materials Physics and Chemistry of the Ministry of Education, Jilin Normal University, Siping* 136000, *China*
[2] *State Key Laboratory of Superhard Materials, Jilin University, Changchun* 130012, *China*

(Received 22 August 2016; revised manuscript received 30 September 2016; published online 10 December 2016)

Improving the thermal stability of diamond and other superhard materials has great significance in various applications. Here, we report the synthesis and characterization of bulk diamond–cBN–B_4C–Si composites sintered at high pressure and high temperature (HPHT, 5.2 GPa, 1620–1680 K for 3–5 min). The results show that the diamond, cBN, B_4C, B_xSiC, SiO_2 and amorphous carbon or a little surplus Si are present in the sintered samples. The onset oxidation temperature of 1673 K in the as-synthesized sample is much higher than that of diamond, cBN, and B_4C. The high thermal stability is ascribed to the covalent bonds of B–C, C–N, and the solid-solution of B_xSiC formed during the sintering process. The results obtained in this work may be useful in preparing superhard materials with high thermal stability.

Keywords: high pressure and high temperature, diamond–cBN–B_4C–Si, composites, high thermal stability

PACS: 81.05.Uj, 81.20.Ev, 81.70.Pg **DOI:** 10.1088/1674-1056/26/1/018102

1. Introduction

Superhard materials such as diamond, cubic boron nitride (cBN), and boron carbide (B_4C) have important applications in the oil, geology, aviation, machinery, metallurgy, and electronics fields.[1–7] However, single-crystal diamond has poor thermal stability (953 K) in ambient atmospheres containing oxygen and lacks chemical inertness with iron system materials. Although cBN has excellent heat resistance (1376 K) and chemical inertness, its hardness (50 GPa) is only half that of diamond (60–120 GPa),[8,9] and corresponding values are lower for commercially used polycrystalline cBN and diamond (PCD), which include metal binders.[10] The hardness of B_4C, which has a diamond structure, is second only to diamond and cBN, and it retains a constant high-temperature hardness (> 30 GPa). However, the poor antioxidant capacity of B_4C (873 K) limits its applicability.[11] Thus, it is of great significance to identify new superhard materials that have outstanding all-round performance and overcome the limitations of diamond, cBN, and B_4C.[8–28]

To date, many studies have focused on improving the thermal stability of diamond and other superhard materials. For example, the onset oxidation temperature in air of the translucent bulk diamond–cBN alloy synthesized at 19 GPa/2300 K reaches 1070 K,[10] whereas that of nanotwinned diamond synthesized at 20 GPa/2273 K reaches 1253 K.[12] This value is above 1600 K, corresponding to unique superhard aggregated boron nitride nanocomposites (ABNNCs).[18] Values of 1525 K[8] and 1567 K[13] have been obtained in submicron cBN compacts sintered at 8 GPa/2300 K and nanotwinned cBN synthesized at 15 GPa/2073 K, respectively, which are higher than those obtained in single-crystal cBN (1376 K), nanograined cBN (1460 K), and commercial polycrystalline cBN (1273 K).[19]

The reported onset oxidation temperature in air for the above materials is attractive, but the conditions needed to prepare these materials are extreme. Thus, it is difficult to apply these materials widely in industry. It is very important to prepare superhard materials with high onset oxidation temperatures in air under moderate conditions (5–6 GPa, 1620–1680 K). Based on the B, C, N, and Si atomic structures and bonding characteristics, they bond with each other more easily in compounds. B_4C is composed of boron and carbon atoms that are mainly combined by covalent bonds, and their atomic radii are close to those of diamond and cBN. The use of B and C atoms in B_4C plays a certain role in forming diamond/cBN composites, and may be expected to improve the thermal stability of the composite. The effects of Si additives for diamond sintering are well known, and the form of SiC within PCD can prevent oxidation of the diamond.[20,21]

In this work, we examine bulk diamond–cBN–B_4C–Si composites prepared at high pressure and high temperature (HPHT, 5.2 GPa, 1620–1680 K for 3–5 min) from the micron-scale raw materials of diamond, cBN, B_4C, and Si. Moreover, the phase structure, surface property, thermal stability, morphology, and sintering mechanism of diamond–cBN–B_4C–Si composites are discussed. Finally, the bonding mechanism for

*Project supported by the National Natural Science Foundation of China (Grant No. 51301075) and the Project of Development and Reform Commission of Jilin Province, China (Grant No. 2014Y136).

†Corresponding author. E-mail: zhupw@jlu.edu.cn
‡Corresponding author. E-mail: lihaibo@jlnu.edu.cn

© 2017 Chinese Physical Society and IOP Publishing Ltd

the superior thermal properties of the composites will be explained.

2. Experiment

2.1. Sample preparation

All specimens were synthesized in an SPD 6×14 MN cubic anvil high-pressure apparatus. The diamond and cBN powders (grain size: 0.5 μm and 0.25 μm, respectively, Henan FeiMeng Co., Ltd., China), B_4C and Si powders (grain size: 2–3 μm and 1 μm, respectively, Shanghai Aladdin Co., Ltd,. China) were used as the starting materials. According to the characteristics of cBN and diamond (high heat resistance and high hardness), the cBN and diamond were used as skeleton materials (85 wt.%). To maintain the hardness of the sintering system, we used as little intermediary material as possible; thus, a little Si (5 wt.%) was used in the sintering system. Based on the above consideration, a mass ratio of 15:70:10:5 was initially used. Firstly, all the powders were mixed for 2 h until smooth, and 2 g of the mixed sample was preloaded at 5 MPa and then heated at 500 °C for 0.5 h for vacuum treatment. Secondly, the raw mixed materials after preloading were placed into a graphite tube, and all components were inserted into a pyrophyllite composite block of 32.5 mm × 32.5 mm × 32.5 mm for the HPHT sintering run. The assembly is shown in Fig. 1. Finally, the samples were kept at 5.2 GPa and 1620–1680 K for 3–5 min, then slowly quenched to room temperature and decompressed to ambient pressure. Diamond–cBN–B_4C–Si composites of 14 mm in diameter and 5.5 mm in thickness were obtained. The temperature was determined from the relation between the temperature and input power, as calibrated using Pt30%Rh–Pt6%Rh thermocouples. The pressure was estimated from the oil press load, which was calibrated by the pressure-induced phase transitions of bismuth (Bi), thallium (Tl), and barium (Ba).

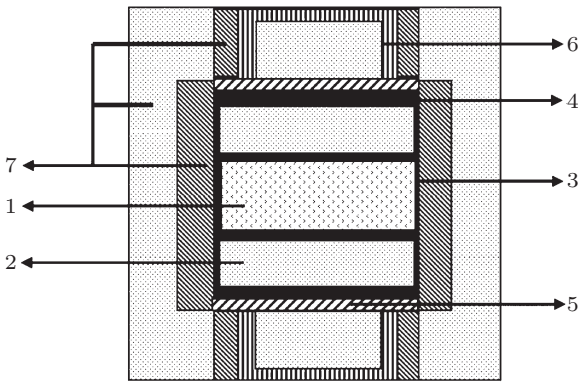


Fig. 1. Schematic diagram of experimental assembly. 1: mixed powders, 2: insulation sheet, 3: graphite heating tube, 4: graphite flake, 5: copper sheet, 6: conductive steel cap, 7: pyrophyllite composite block.

2.2. Sample characterization

To examine the sintering mechanism and properties, all specimens were polished, fractured, and purified for measurements. X-ray diffraction (XRD, Rigaku PC2500, Japan) was used to investigate the phase composition of the samples. The machine was operated at 30 kV and 100 mA using Cu-Kα radiation ($\lambda = 1.5418$ Å) from 20°–90°. Raman analyses of the phase structure were performed using a Raman microscope (Renishaw inVia, UK) with a 514 nm Ar^+ laser in backscattering geometry. The oxidation resistance was studied in air using a simultaneous thermal analyzer (DSC/TG-DTA, NETZSCH STA 449 F5, Germany) with a heating rate of 10 K/min from 300 to 1773 K. The microstructure features were investigated by field emission scanning electron microscopy (FE-SEM, JEOL JSM-7800F, Japan). X-ray photoelectron spectroscopy (XPS, Thermo Fisher ESCALAB250xi, USA) was used to test the surface properties with a monochromatized Al-Kα x-ray as the excitation source.

3. Results and discussion

3.1. Composition and reaction mechanism analysis

3.1.1. Phase structure characterization by XRD

To investigate the form of the components and the reaction mechanism in the sintered system, the starting mixed powders (Fig. 2(a)) and the surface of the composites were characterized by XRD (Figs. 2(b) and 2(c)). Under HPHT conditions, a strong chemical combination occurs among the starting materials according to the reaction

$$\mathrm{B} + \mathrm{Si} + \mathrm{C} \rightarrow \mathrm{B}_x\mathrm{SiC}. \quad (1)$$

Compared to the starting mixed powders (Fig. 2(a)), the diffraction peak intensity of Si changed significantly because of the chemical reaction among Si, B, and C, which generated a stable phase of B_xSiC (see Eq. (1) and Fig. 2(b)). The B and C of B_xSiC are mainly taken from the B_4C, with a small amount coming from the cBN and diamond, respectively, during the sintering process. The cBN and diamond are skeleton hard materials. Additionally, the phases of graphite, SiO_2, and Si from a surplus of starting materials are reflected in the XRD patterns for the synthesis at 5.2 GPa/1680 K for 3 min. With the increase in sintering time, the samples become seriously graphitized, but do not exhibit any remaining Si (Fig. 2(c)). The graphite may be from the decomposition of B_4C at HPHT, rather than from the graphitization of diamond.[22] It can be seen that the relative intensities of the x-ray diffraction peaks for cBN and diamond did not change (Figs. 2(b) and 2(c)). The XRD analysis results also show that the composite material depends on the bonding strength of the combination among cBN, B_4C, and diamond through Si as an intermediary agent. The lattice constants of diamond and cBN in the composites are 3.566 (3.567 in single crystal) and 3.618 (3.616 in single crystal), respectively. This suggests that the formation of composites did not lead to the expansion of the lattice parameters of diamond and cBN.

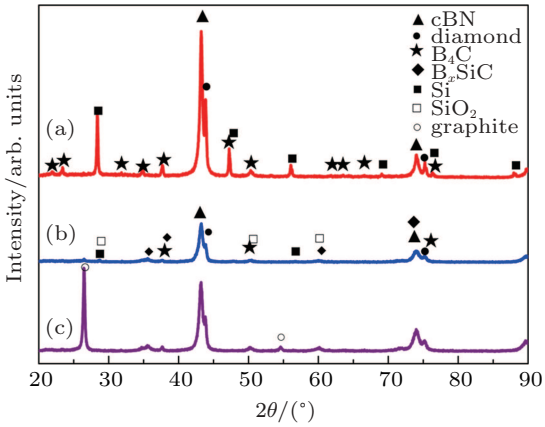


Fig. 2. (color online) XRD patterns for the starting mixed powders and diamond–cBN–B_4C–Si samples: (a) the starting mixed powders, (b) the sample synthesized at 5.2 GPa/1680 K for 3 min, and (c) the sample synthesized at 5.2 GPa/1620 K for 5 min.

3.1.2. Phase structure characterization by Raman spectroscopy

As shown in Figs. 3(a) and 3(b), weak Raman shifts occurred in the cBN (1059 cm^{-1} and 1310 cm^{-1}). Nanophase graphite and amorphous carbon (peak of 1357 cm^{-1}) were also found within the samples,[29,30] possibly from the decomposition of B_4C at HPHT rather than the graphitization of diamond. The peaks of 1583 cm^{-1} and 1622 cm^{-1}also indicate that the original C from B_4C had changed, forming the graphite and amorphous carbon. The analyses of the graphitization by XRD and Raman are consistent.

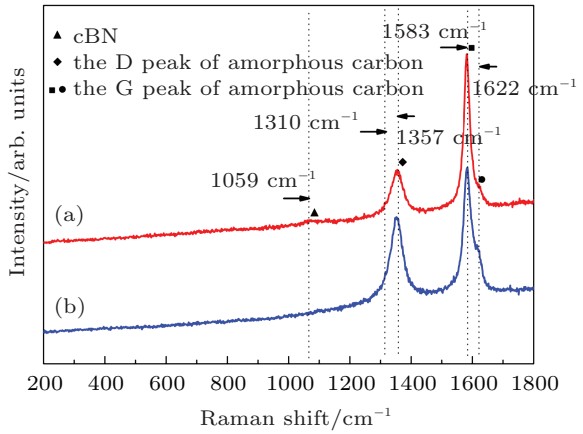


Fig. 3. (color online) Raman spectra characterization of the samples (a) sintered at 5.2 GPa/1680 K for 3 min and (b) sintered at 5.2 GPa/1620 K for 5 min.

3.2. Oxidation resistance and microstructure morphology tests

3.2.1. Oxidation resistance characterization

The thermal stability (oxidation resistance) measurement for diamond–cBN–B_4C–Si bulk samples was performed using a simultaneous thermal analyzer (DSC/TG-DTA) in air, shown in Figs. 4(a) and 4(b). The onset oxidation temperature of 1673 K (Fig. 4(a)) was established from the thermal gravimetric curves. This is higher than that of PCD (869 K), polycrystalline cBN (PcBN) (1273 K), SiC (1273 K), and diamond–cBN alloys (1070 K).[10] As the sintering time increased, the composite material became mildly burnt, resulting in heat-resistant performance down to1663 K, shown in Fig. 4(b).

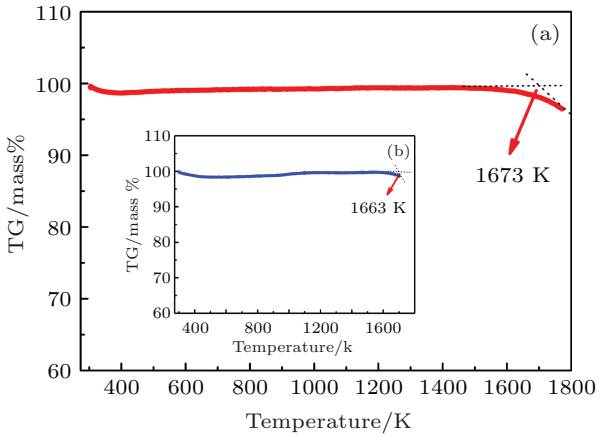


Fig. 4. (color online) Thermo-gravimetric (TG) curves for a diamond–cBN–B_4C–Si bulk samples (a) sintered at 5.2 GPa/1680 K for 3 min and (b) sintered at 5.2 GPa/1620 K for 5 min.

3.2.2. Microstructure morphology characterization by FE-SEM

To clarify the microstructure morphology, the cross-sectional layer of the specimens was observed by means of FM-SEM. The cross-sectional microstructures of sintered diamond–cBN–B_4C–Si composites under different conditions are presented in Figs. 5(a)–5(d). There are many big particles in the sample sintered at 5.2 GPa/1620 K for 3 min, and little bonding has formed between the particles (Fig. 5(a)). As the sintering time increased, the large-area bonding structures began to form and become denser (Fig. 5(b)). As shown in Fig. 5(c), after HTHP, parts of the initial diamond, cBN, and B_4C particles had grown bigger and formed a large area of adhesive flake structure morphology exhibiting a transgranular fracture mode. It is considered that a dense and interlaced microstructure with diamond–diamond (D–D), BN–BN, and diamond–BN–SiC direct bonding had formed in the diamond–cBN–B_4C–Si. Furthermore, the average grain size is about 100 nm and uniform (Fig. 5(d)). Hence, there must be more grain boundary for the fine grain size in the as-synthesized composites. This result may be useful for enhancing the thermal stability.[8]

3.3. Surface property and high thermal stability mechanism characterization by XPS

3.3.1. Surface property characterization

To better explain the high thermal stability mechanism, XPS measurements were taken to determine the chemical

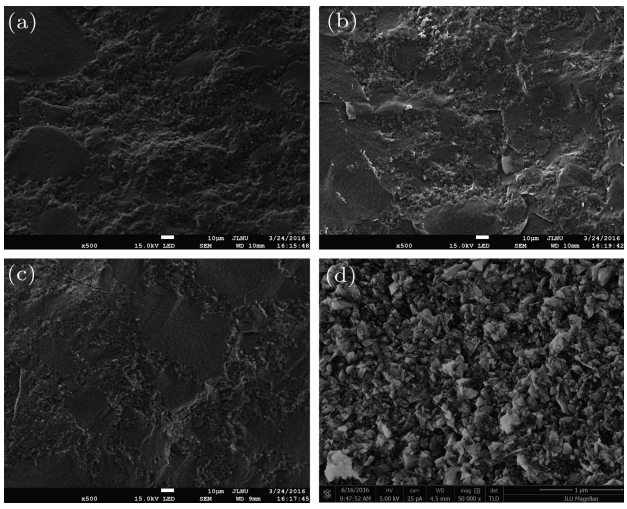


Fig. 5. FM-SEM characterization of the samples (a) sintered at 5.2 GPa/1620 K for 3min, (b) sintered at 5.2 GPa/1620 K for 5 min, (c) sintered at 5.2 GPa/1680 K for 3 min. (d) 100 times of panel (c).

state and surface properties of the powders from the broken samples. The results are shown in Fig. 6. These measurements reveal chemical bonds of B–Si, C–N, and Si–C (but not C–C and B–N), presumably formed in diamond–cBN–B_4C–Si (Figs. 6(a)–6(d)). The main deconvolution peak of the B 1s spectrum for diamond–cBN–B_4C–Si sintered at 5.2 GPa/1680 K for 3 min is located at 190.9 eV (Fig. 6(a)), which is the B 1s binding energy of the B–N bond in cBN (190.9 eV).[31–33] A lower binding energy of 187.9 eV for B 1s suggests a contribution from the bonding configurations between B and Si, which correspond to the B–Si bond in SiC. This indicates that B atoms have been incorporated into the SiC lattice and substituted at Si sites, generating a solid-solution of B_xSiC and becoming uniformly distributed in the sample, which is consistent with a previous report.[34] The existence of a high-temperature boundary phase in the B_xSiC shows that the starting materials of cBN, B_4C, and diamond reacted solidly with one another. The C 1s spectrum (Fig. 6(b)) demonstrates the presence of C–N and C–B bonds in the diamond–cBN–B_4C–Si, in addition to the dominant C–C bonds in diamond.[8] The N 1s XPS spectrum (Fig. 6(c)) further confirms that the bond between N and B is the binding energy of the B–N bond in cBN (398.3 eV). From the XPS spectra of Si 2p (Fig. 6(d)), the peak centered at 100.5 eV (near 100.7 eV) corresponds to the Si–C bond in SiC.[35] The contribution from the Si–O bond in SiO_2 is attributed to the Si–O reaction at the surface of the sample due to air exposure.

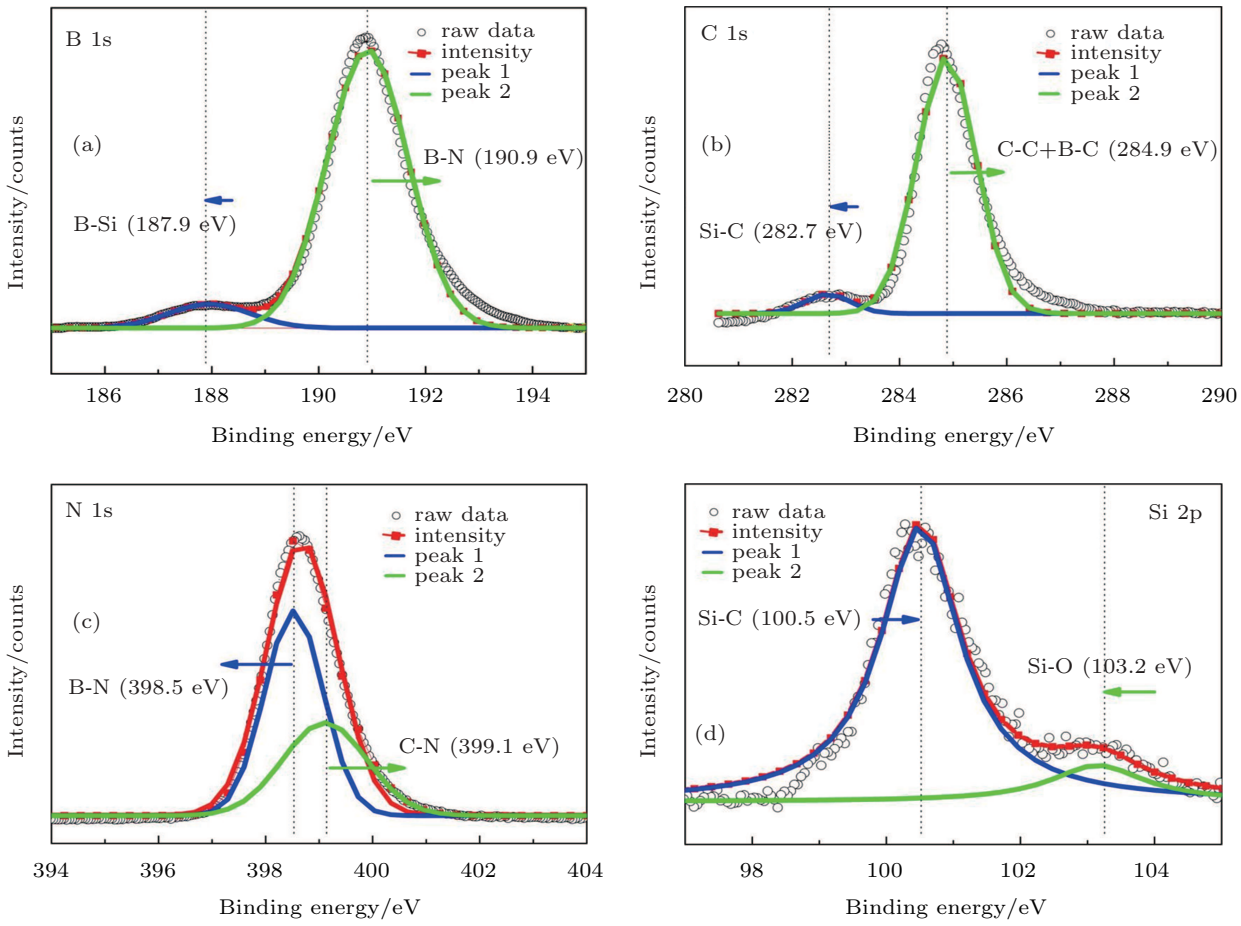


Fig. 6. (color online) XPS analysis of the recovered diamond–cBN–B_4C–Si sample. (a)–(d) XPS spectra for B 1s, C 1s, N 1s, and Si 2p core levels for the sample synthesized at 5.2 GPa/1680 K for 3 min. A combination of Gaussian and Lorentzian were used in the fitting of observed spectra. Different binding energies for each element suggest multiple bonding in the sample.

3.3.2. High thermal stability mechanism analyses

The covalent bonds of B–C, C–N, and Si–C revealed by XPS strongly suggest that a solid-solution reaction among diamond, cBN, and B_4C takes place during the sintering process at HPHT, most likely at or near the grain boundaries. Furthermore, these processes, similar to those that made an exceptional antioxidant material through B–C–N–Si ternary phases, help to enhance the thermal stability and mechanical properties, such as reducing the stress of crystallization, further enhancing the adhesion of grain boundaries, and maintaining a high wear resistance.[10,15,36] Moreover, the silicon oxides (SiO_2) prevent further oxidation of the interior of the composites in the process of high-temperature oxidation. In a thermogravimetric curve, therefore, the front exhibits no change.

4. Conclusion

Diamond–cBN–B_4C–Si composites with high thermal stability have been successfully prepared under relatively low temperature and pressure conditions (5.2 GPa, 1620–1680 K for 3–5 min). The TGA result shows that the onset oxidation temperature of 1673 K for diamond–cBN–B_4C–Si composite is much higher than that of the starting materials, including diamond, cBN, and B_4C. The mechanism of the high thermal stability is explained by the covalent bonds of B–C, C–N, Si–C and the solid-solution of B_xSiC and SiO_2 that exist in the sintered samples.

References

[1] Bovenkerk H P, Bundy F P, Hall H T, Strong H M and Wentorf R H 1959 *Nature* **184** 1094
[2] Altukhov A A, Afanas'ev M S, Kvaskov V B, Lyubchenko V E, Mityagin Y A, Murav'ev E N, Pomortsev L A, Potapov V A and Spitsyn B V 2004 *Inorg. Mater.* **40** 50
[3] Koizumi S, Watanabe K, Hasegawa M and Kanda H 2001 *Science* **292** 1899
[4] Ekimov E A, Sidorov V A, Bauer E D, Mel'nik N N, Curro N J, Thompson J D and Stishov S M 2004 *Nature* **428** 542
[5] Tillmann W 2000 *Int. J. Refract. Met. Hard Mater.* **8** 301
[6] Tian Y, Xu B and Zhao Z 2012 *Int. J. Refract. Met. Hard Mater.* **33** 93
[7] Xu B and Tian Y 2015 *Sci. China-Mater.* **58** 132
[8] Wang P, He D W, Wang L P, Kou Z L, Li Y, Lun X, Hu Q W, Xu C, Li L, Wang Q M, Liu J and Zhao Y S 2015 *Appl. Phys. Lett.* **107** 101901
[9] Solozhenko V L, Kurakevych O O and Godec Y L 2012 *Adv. Mater.* **24** 1540
[10] Liu G D, Kou Z L, Yan X Z, Li L, Fang P, Wang Q M, Wang K X, Wang P, Liang L, Li Y, Li W T, Wang Y H, Yan B, Yang L and He D W 2015 *Appl. Phys. Lett.* **106** 121901
[11] Badzian A R 1988 *Appl. Phys. Lett.* **53** 2495
[12] Huang Q, Yu D L, Xu B, Hu W T, Ma Y M, Wang Y B, Zhao Z S, Wen B, He J L, Liu Z Y and Tian Y J 2014 *Nature* **510** 250
[13] Tian Y J, Xu B, Yu D L, Ma Y M, Wang Y B, Jiang Y B, Hu W T, Tang C C, Gao Y F, Luo K, Zhao Z S, Wang L M, Wen B, He J L and Liu Z Y 2013 *Nature* **493** 385
[14] Solozhenko V L, Andrault D, Fiquet G, Mezouar M and Rubie D C 2001 *Appl. Phys. Lett.* **78** 1385
[15] Xu C, He D W, Wang H K, Wang W D, Tang M J and Wang P 2014 *Chin. Sci. Bull.* **59** 5251
[16] Tang M J, He D W, Wang W D, Wang H K, Xu C, Li F J and Guan J W 2012 *Scripta Mater.* **66** 781
[17] Luo X G, Zhou X F, Liu Z Y, He J L, Xu B, Yu D L, Wang H T and Tian Y J 2008 *J. Phys. Chem. C* **112** 9516
[18] Dubrovinskaia N, Solozhenko V L, Miyajima N, Dmitriev V, Kurakevych O O and Dubrovinsky L 2007 *Appl. Phys. Lett.* **90** 101912
[19] Sumiya H, Uesaka S and Satoh S 2000 *J. Mater. Sci.* **35** 1181
[20] Qian J, Voronin G, Zerda T W, He D and Zhao Y 2002 *J. Mater. Res.* **17** 2153
[21] Qian J, He D, Daemen L and Zhao Y 2003 *J. Mater. Res.* **18** 1173
[22] Cui H Z, Liu W, Cao L L, Song Q, Tian J, Teng F L and Wang J 2015 *J Euro. Cera. Soci.* **35** 3381
[23] Dub S N and Petrusha I A 2006 *High Pressure Res.* **26** 71
[24] Irifune T, Kurio A, Sakamoto S, Inoue T and Sumiya H 2003 *Nature* **421** 599
[25] Zhao Y C and Wang M Z 2008 *J. Mater. Process. Tech.* **198** 134
[26] Kaner R B, Gilman J J and Tolbert S H 2005 *Science* **308** 1268
[27] Li Y, Zhou Z X, Guan X M, Li S S, Wang Y, Jia X P and Ma H A 2016 *Chin. Phys. Lett.* **33** 28101
[28] Li W S, Zhang J, Dong H F, Zhu K, Wang S C, Liu Y and Li Y M 2013 *Chin. Phys. B* **22** 018102
[29] Obraztsov A N, Timofeyev M A, Guseva M B, Babaev V G, Valiulova Z K and Babina V M 1995 *Diam. Relat. Mater.* **4** 968
[30] Prawer S and Nemanieh R J 2004 *Phil. Trans. R. Soc. Lond. A* **362** 2537
[31] Liu X B, Jia X P, Zhang Z F, Zhao M, Guo W, Huang G F and Ma H A 2011 *Cryst. Growth Des.* **11** 1006
[32] Ci L, Song L, Jin C, Jariwala D, Wu D, Li Y, Srivastava A, Wang Z F, Storr K, Balicas L, Liu F and Ajayan P M 2010 *Nat. Mater.* **9** 430
[33] Watanabe M O, Itoh S, Mizushima K and Sasaki T 1996 *Appl. Phys. Lett.* **68** 2962
[34] Oswald S and Wirth H 1999 *Surf. Interface Anal.* **27** 136
[35] Dong L L, Wang Y Y, Tong X L, Jin G Q and Guo X Y 2014 *Acta. Phys. -Chim. Sin.* **30** 135
[36] Wang H K, He D W, Xu C, Tang M J, Li Y, Dong H N, Meng C M, Wang Z G and Zhu W J 2013 *J. Appl. Phys.* **113** 043505